Appendix A: Bootstrap Stability Figures

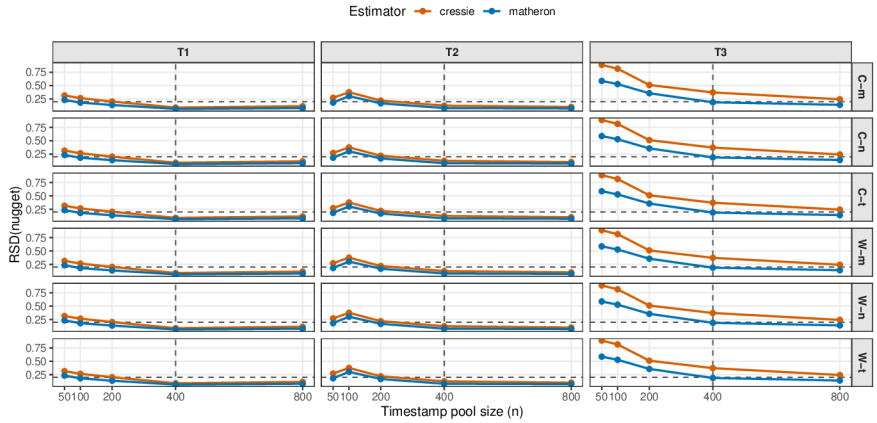

FIGURE A.1: Bootstrap stability diagnostics of the nugget parameter for the Agriculture landscape.

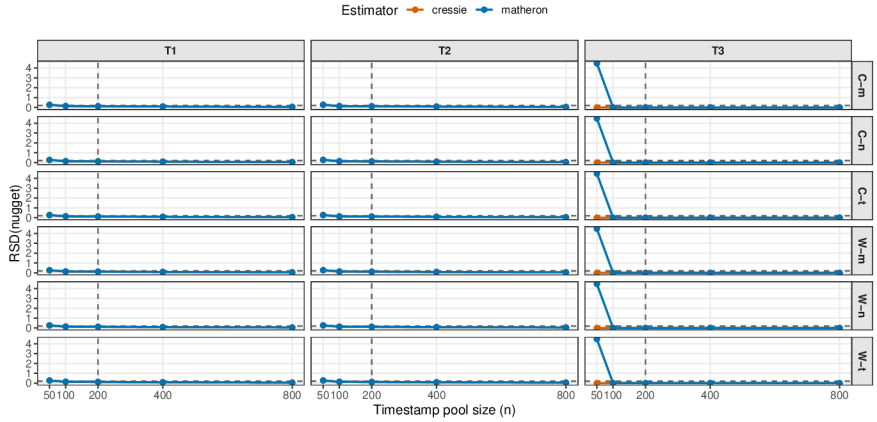

FIGURE A.2: Bootstrap stability diagnostics of the nugget parameter for the Drainage landscape.

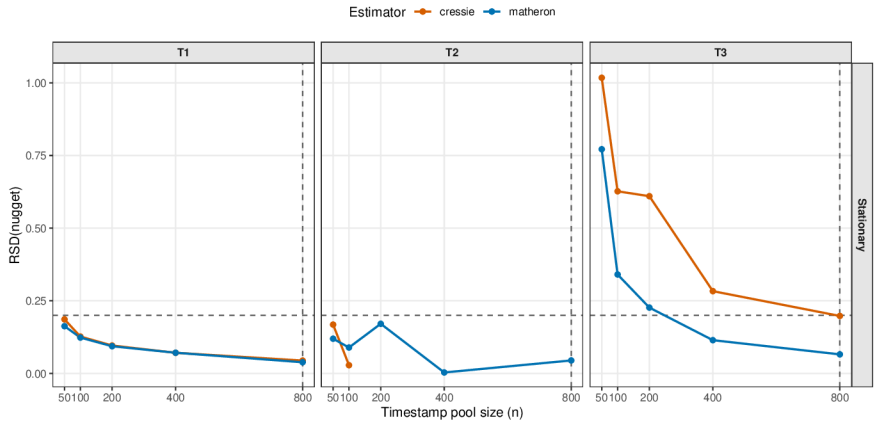

FIGURE A.3: Bootstrap stability diagnostics of the nugget parameter for the KL landscape.

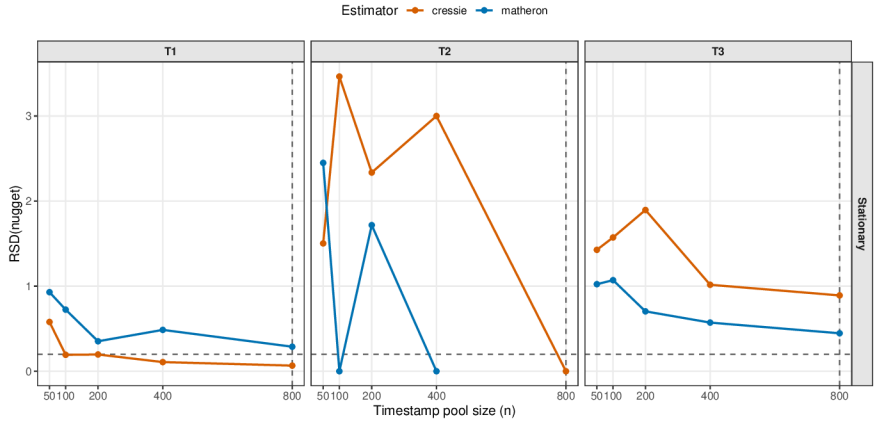

FIGURE A.4: Bootstrap stability diagnostics of the nugget parameter for the BP landscape.

Appendix B: Additional Variogram Models

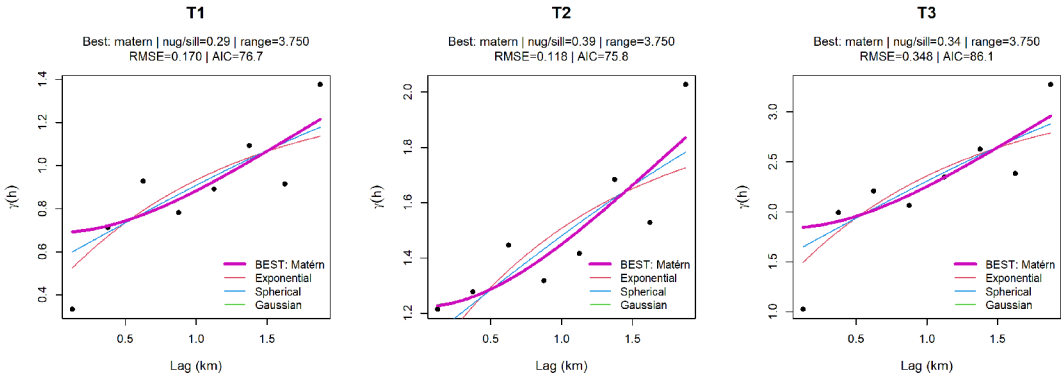

FIGURE B.1: Representative variogram model fits for the Agriculture landscape during the warm-transition regime.

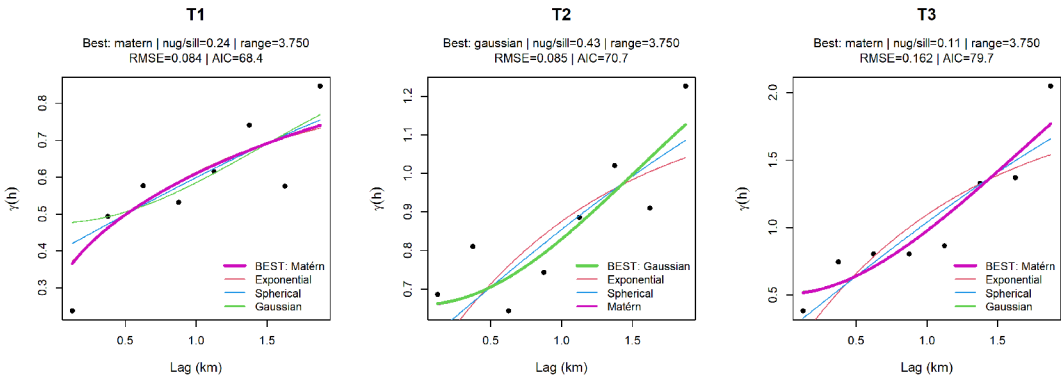

FIGURE B.2: Representative variogram model fits for the Agriculture landscape during the warm-night regime.

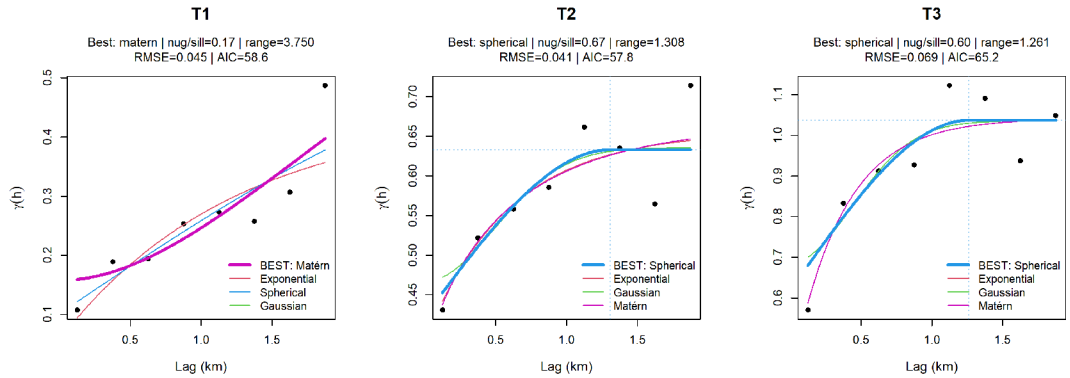

FIGURE B.3: Representative variogram model fits for the Agriculture landscape during the cold-midday regime.

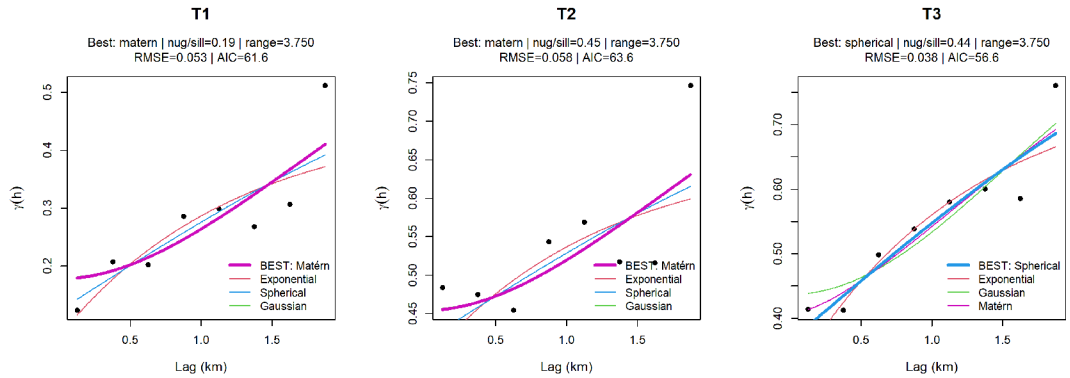

FIGURE B.4: Representative variogram model fits for the Agriculture landscape during the cold-transition regime.

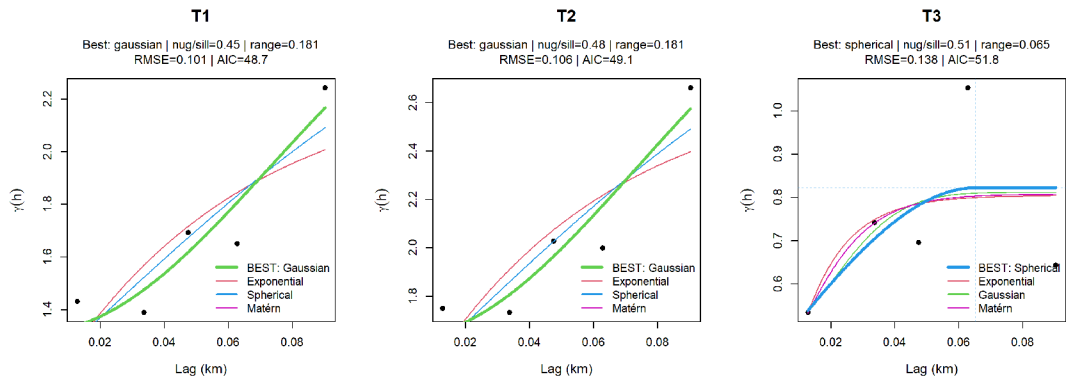

FIGURE B.5: Representative variogram model fits for the Drainage landscape during the warm-transition regime.

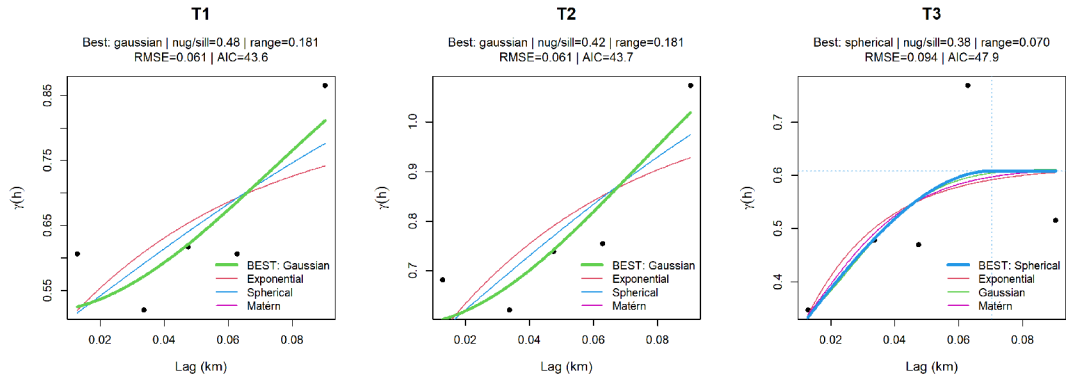

FIGURE B.6: Representative variogram model fits for the Drainage landscape during the warm-night regime.

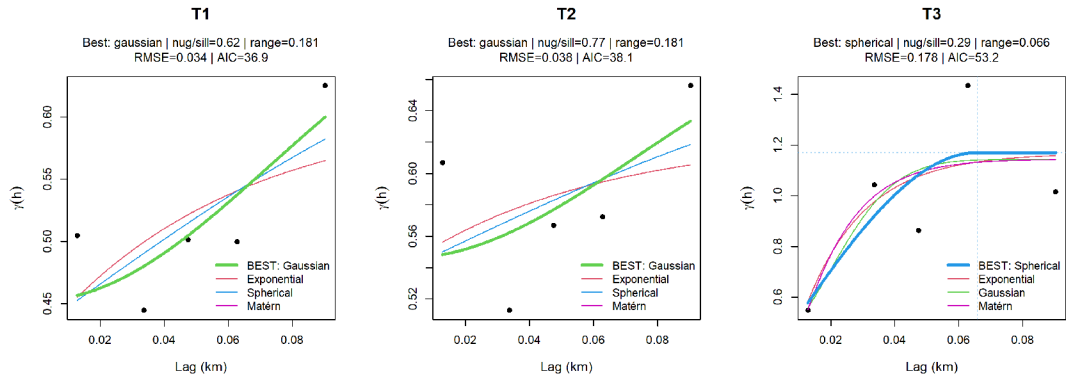

FIGURE B.7: Representative variogram model fits for the Drainage landscape during the cold-midday regime.

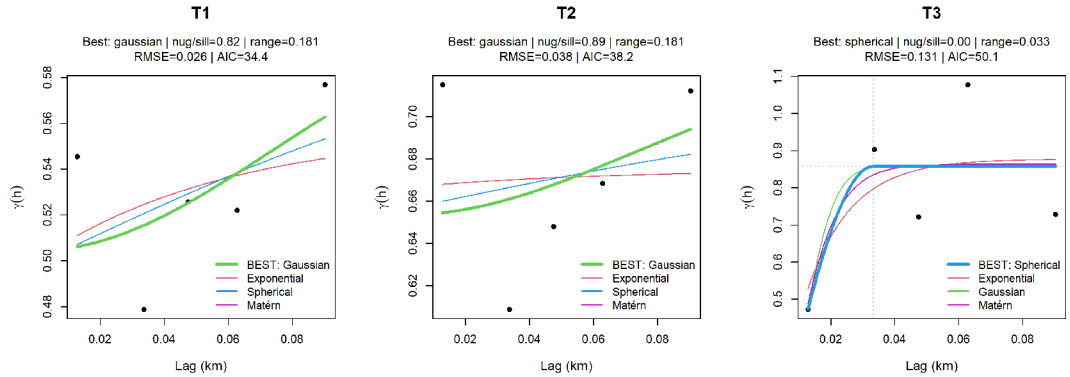

FIGURE B.8: Representative variogram model fits for the Drainage landscape during the cold-transition regime.

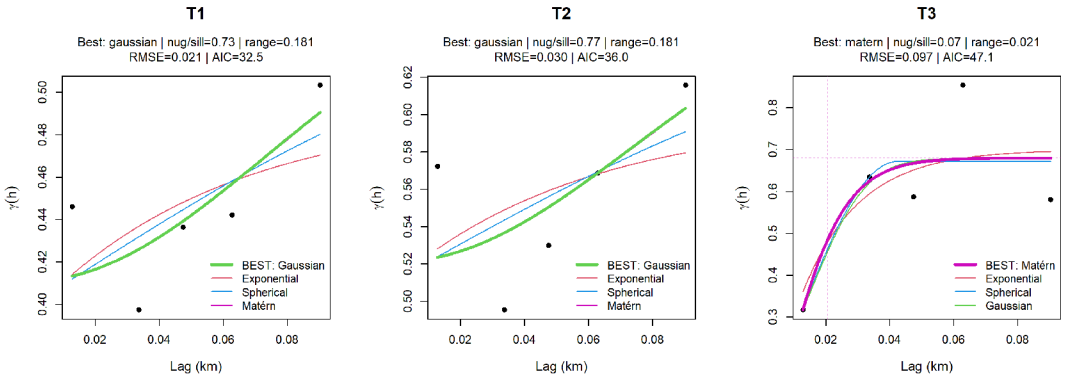

FIGURE B.9: Representative variogram model fits for the Drainage landscape during the cold-night regime.

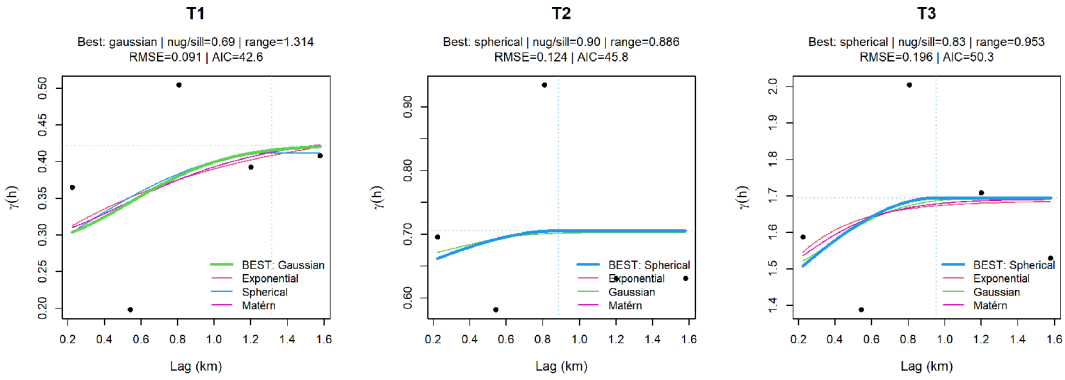

FIGURE B.10: Representative variogram model fits for the KL landscape under stationary conditions.

Appendix C: Additional Spatial Interpolation Maps

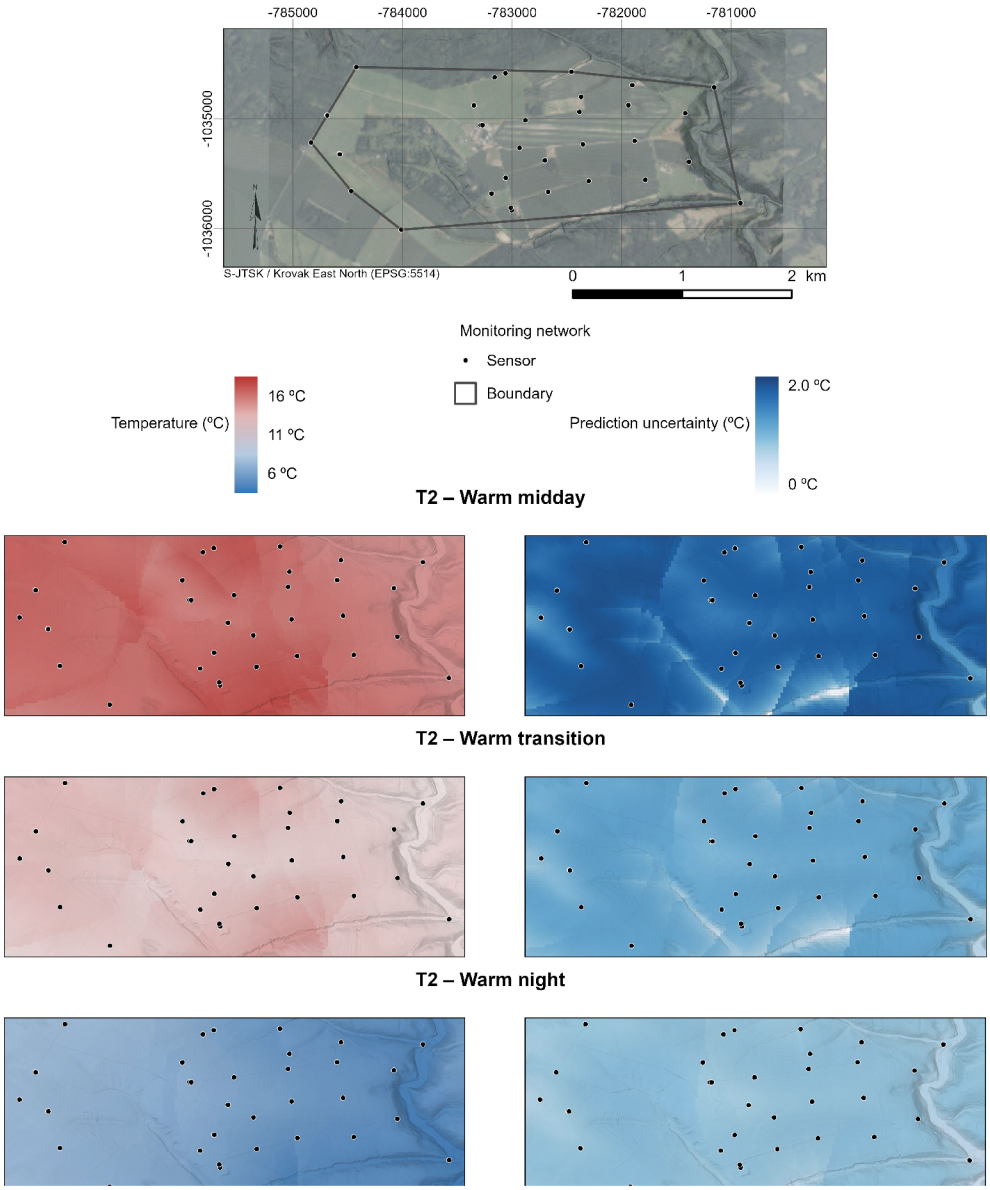

FIGURE C.1: Spatial prediction of subsurface (soil) temperature (T2) for three representative regimes (warm-midday, warm-transition, and warm-night) in the Agriculture landscape using KED, with DEM-derived elevation as the drift variable. Left panels show predicted temperature, and right panels show the associated prediction standard deviation. A common color scale is used across all regimes for both temperature and uncertainty to allow direct comparison.

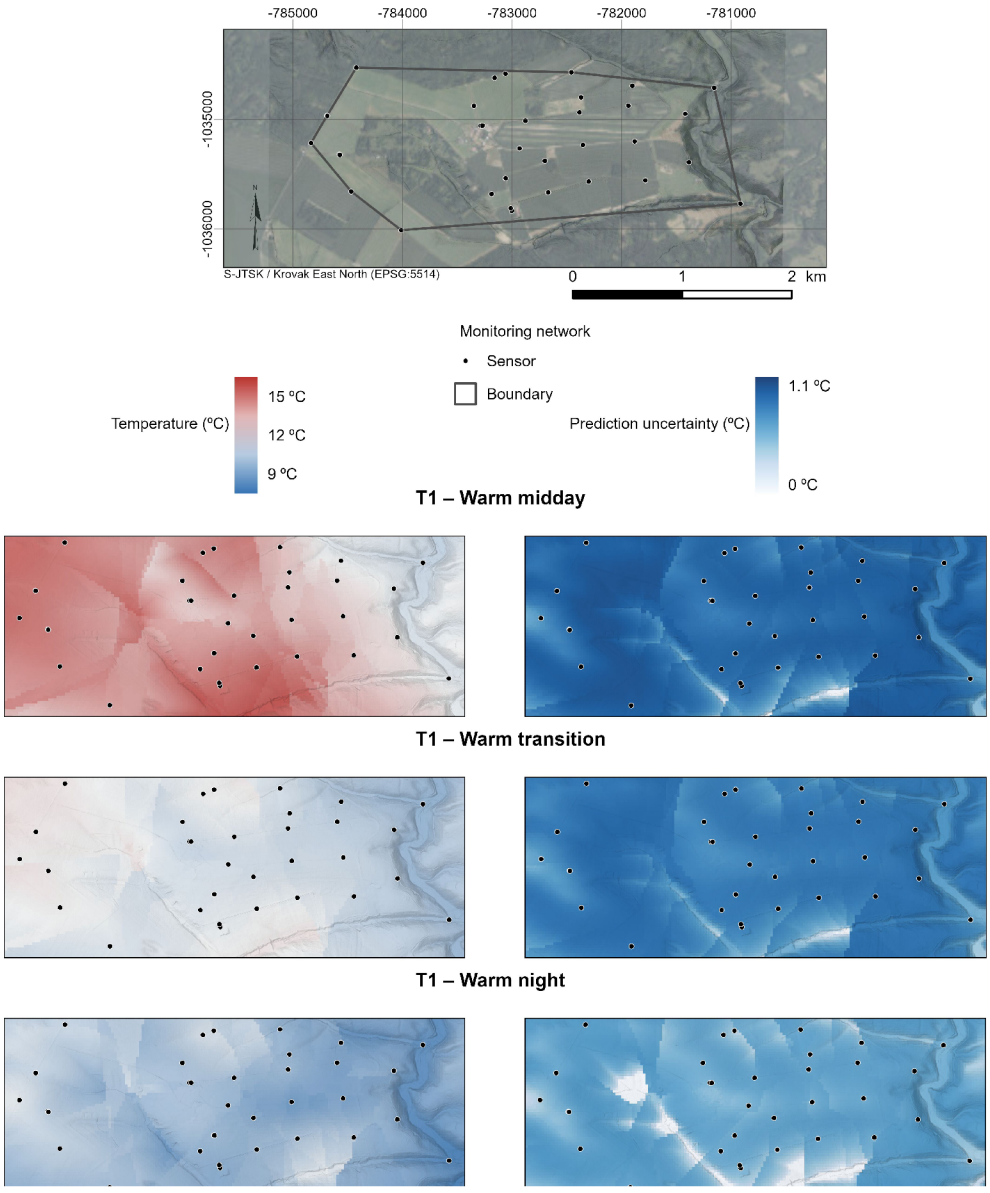

FIGURE C.2: Spatial prediction of deeper soil temperature (T1) for three representative regimes (warm-midday, warm-transition, and warm-night) in the Agriculture landscape using KED, with DEM-derived elevation as the drift variable. Graphical conventions follow those described in Figure C.1.

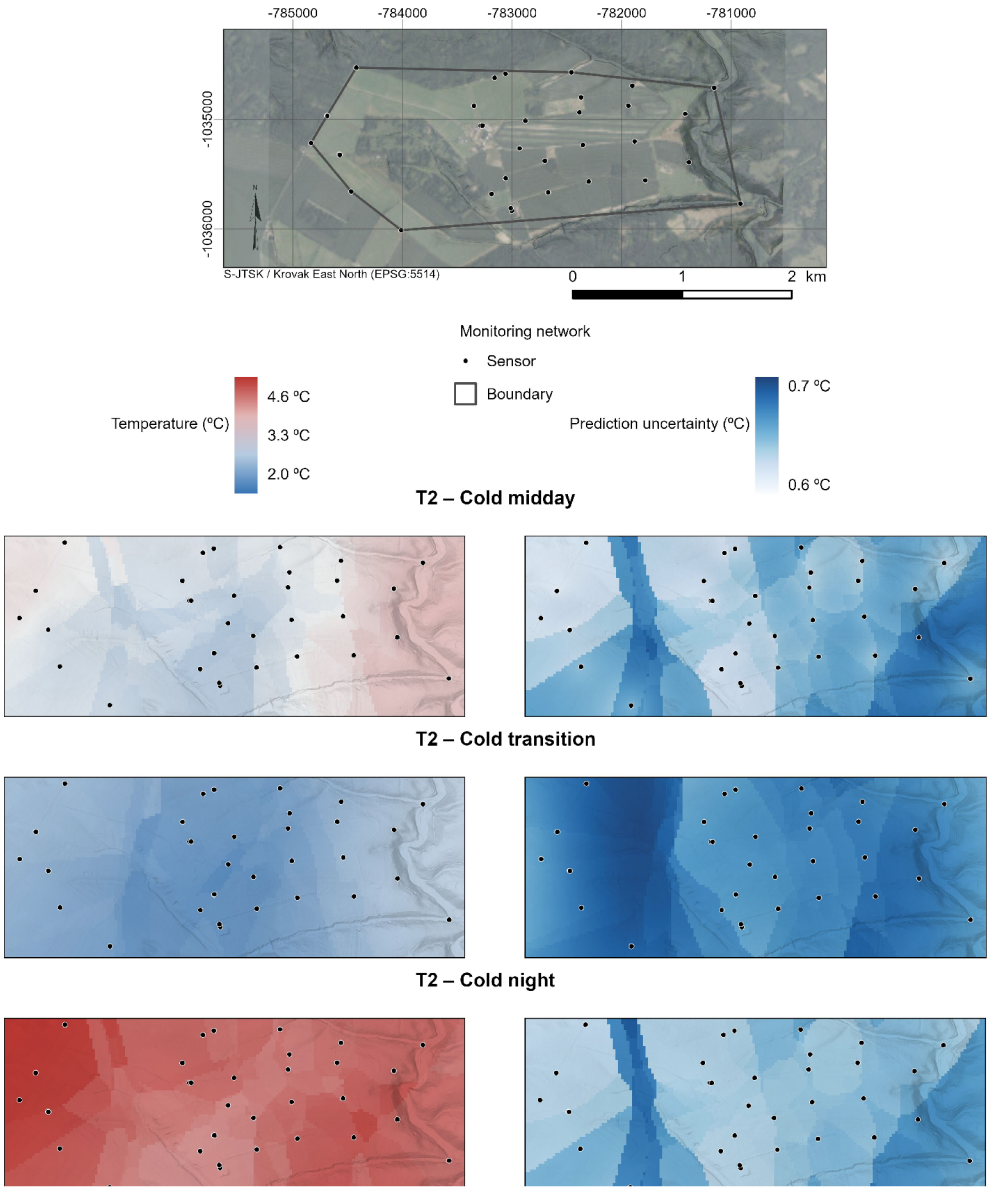

FIGURE C.3: Spatial prediction of subsurface (soil) temperature (T2) for three representative regimes (cold-midday, cold-transition, and cold-night) in the Agriculture landscape using OK. Graphical conventions follow those described in Figure C.1.

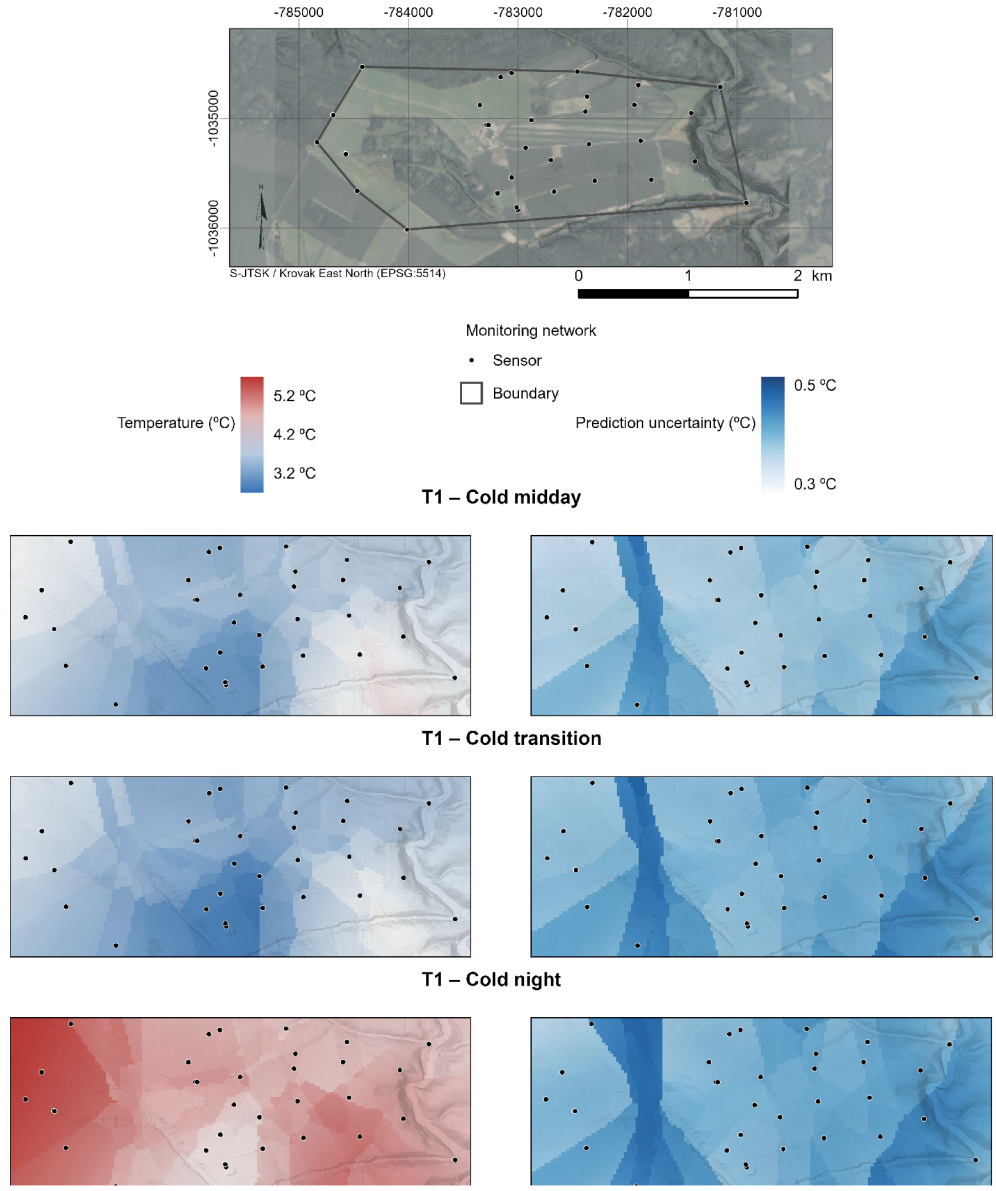

FIGURE C.4: Spatial prediction of deeper soil temperature (T1) for three representative regimes (cold-midday, cold-transition, and cold-night) in the Agriculture landscape using OK. Graphical conventions follow those described in Figure C.1.

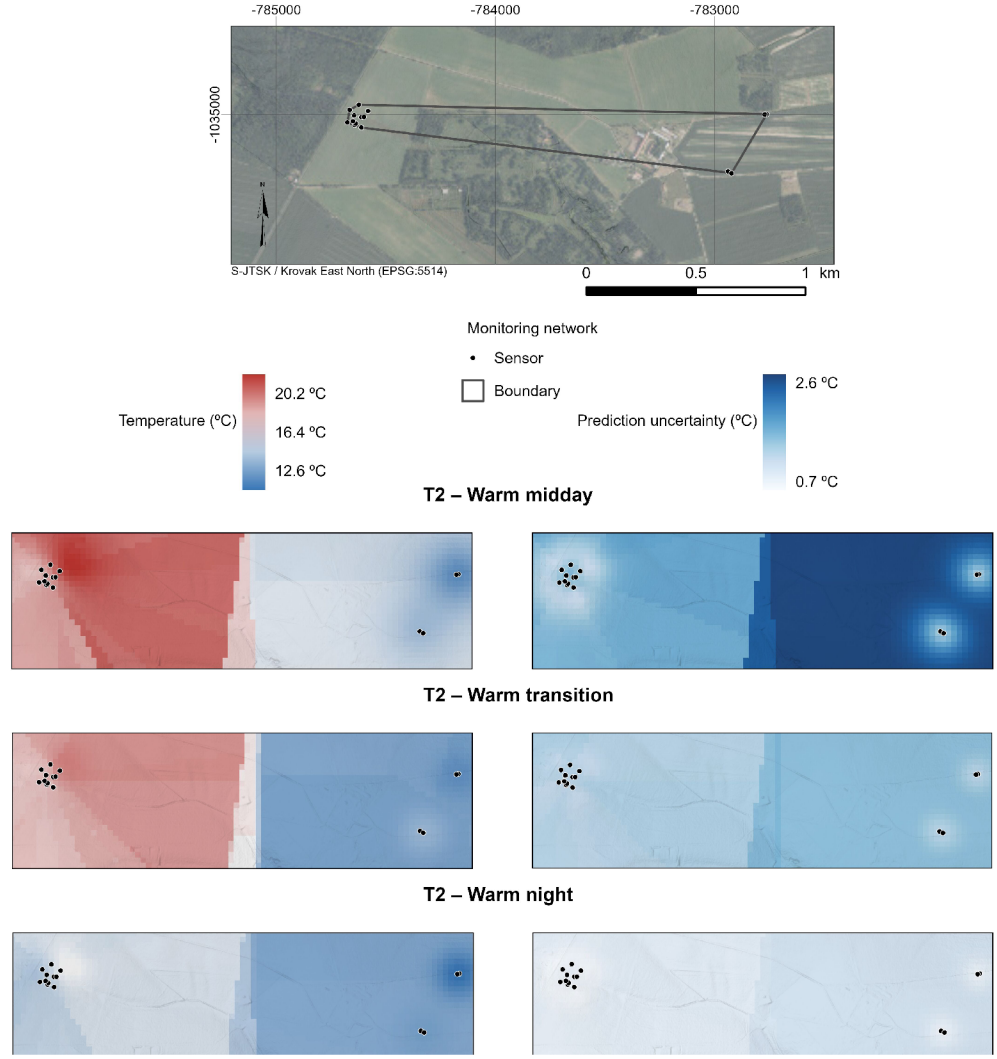

FIGURE C.5: Spatial prediction of subsurface (soil) temperature (T2) for three representative regimes (warm-midday, warm-transition, and warm-night) in the Drainage landscape using OK. Graphical conventions follow those described in Figure C.1.

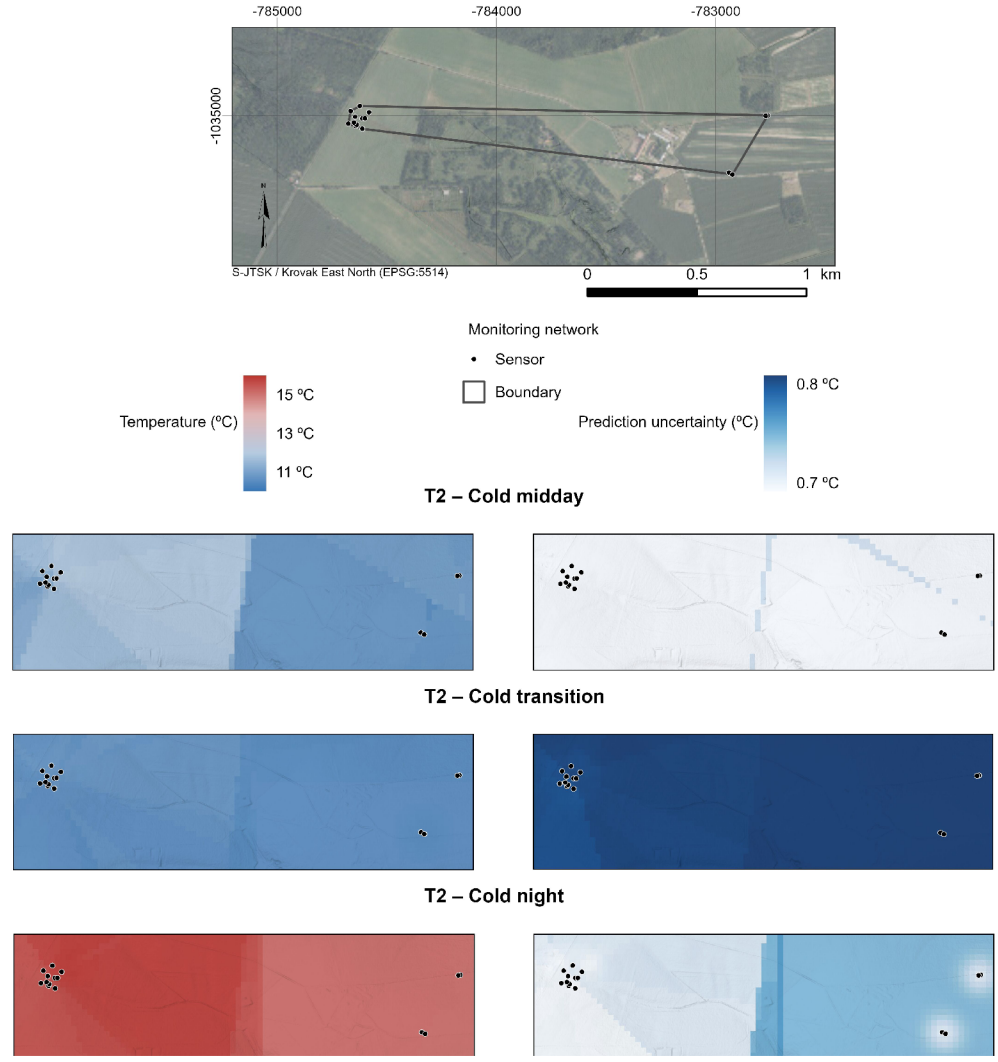

FIGURE C.6: Spatial prediction of subsurface (soil) temperature (T2) for three representative regimes (cold-midday, cold-transition, and cold-night) in the Drainage landscape using OK. Graphical conventions follow those described in Figure C.1.

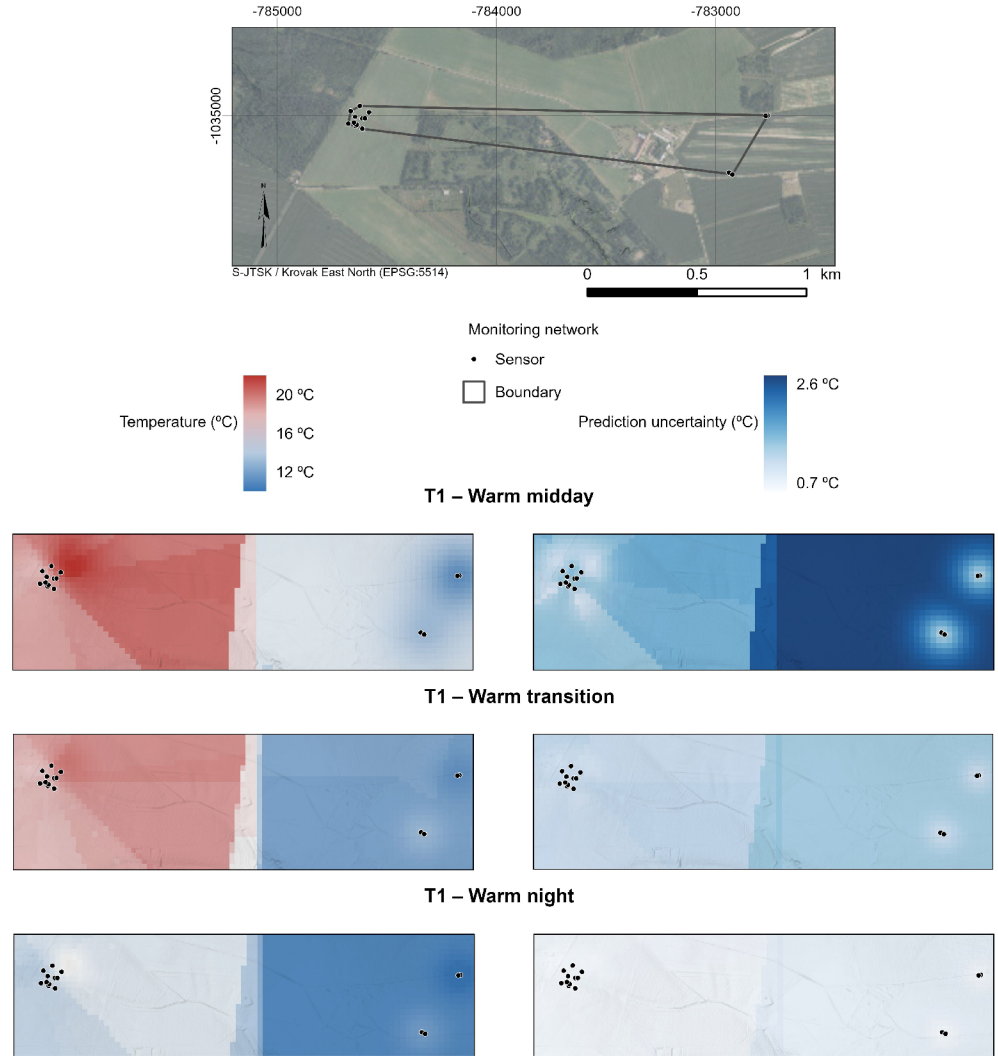

FIGURE C.7: Spatial prediction of deeper soil temperature (T1) for three representative regimes (warm-midday, warm-transition, and warm-night) in the Drainage landscape using OK. Graphical conventions follow those described in Figure C.1.

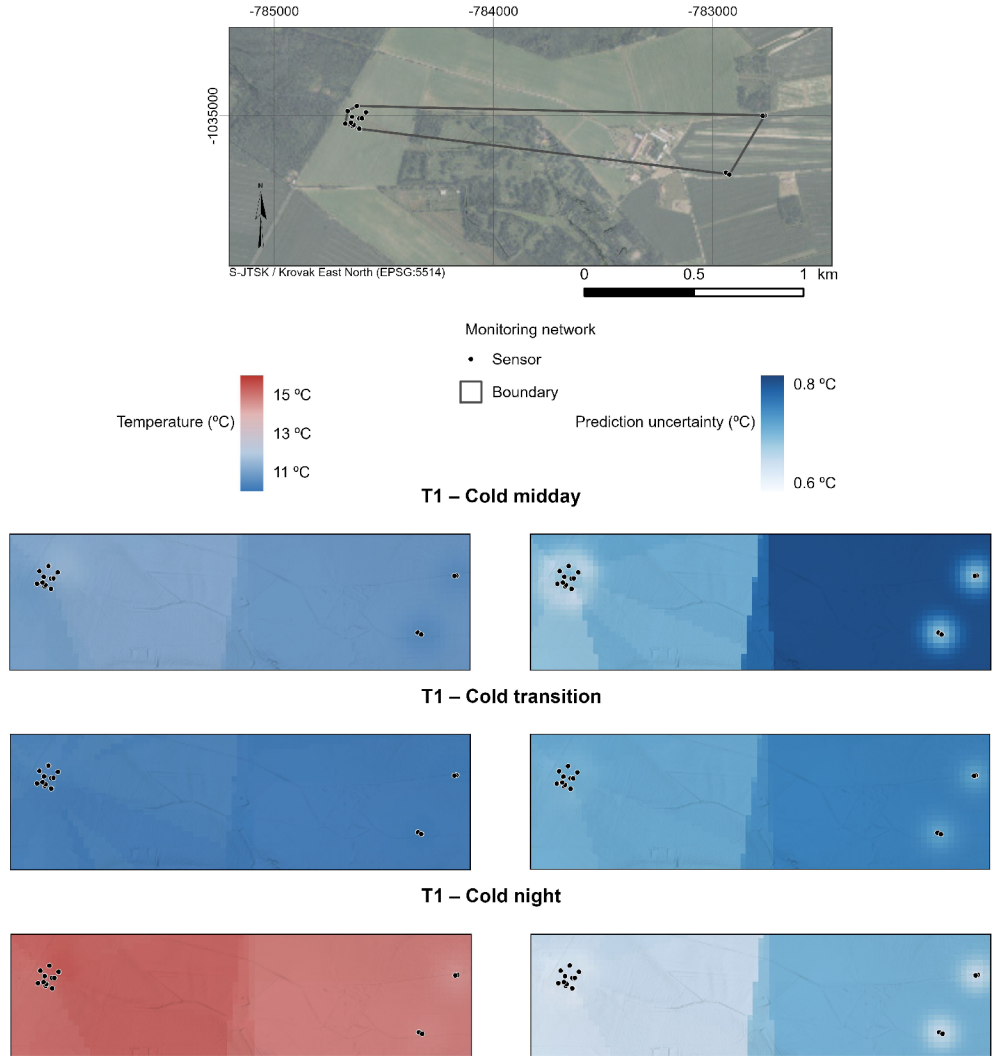

FIGURE C.8: Spatial prediction of deeper soil temperature (T1) for three representative regimes (cold-midday, cold-transition, and cold-night) in the Drainage landscape using OK. Graphical conventions follow those described in Figure C.1.